Materials Science & Engineering A 697 (2017) 203–210

Contents lists available at ScienceDirect

Materials Science & Engineering A

journal homepage: www.elsevier.com/locate/msea

High temperature deformation behavior of as-produced and retired 9–12% Cr power plant steel

Magdy M. El Rayes[a], Ehab A. El-Danaf[a,b,*]

[a] Mechanical Engineering Department, College of Engineering, King Saud University, P.O. Box 800, 11421 Riyadh, Saudi Arabia
[b] Department of Mechanical Design and Production, Faculty of Engineering, Cairo University, Egypt

ARTICLE INFO

Keywords:
Martensitic steel
High temperature tensile test
Strain rate
Activation energy
Stress exponent

ABSTRACT

This work aims to compare and analyze the high temperature behavior of as-received and retired 9–12% Cr steel, at high temperatures to elucidate the dominant deformation mechanism. The retired material was selected from retired shrouds used at the third stage of gas-turbine power plant which served for 30,000 h. at about 550–600 °C (823–873 K). High temperature tensile testing in the range of 813–933 °K and different strain rates of 1×10^{-3} to 1×10^{-5} s^{-1}, were conducted on the two material conditions. The microstructural characterization showed that both microstructures were typical tempered martensite composed of large prior austenite grains containing martensite laths as well as occasional ferrite islands. EBSD was used to reveal grain characteristics for the two material conditions. The deformation was found to be controlled by low temperature climb. This was confirmed by the values of true activation energies which were close to 60% of lattice diffusion of ferrite for both material conditions. This inference was concealed by the presence of threshold stresses that initiated due to the interaction of dislocations with carbides. The data was consolidated using the Zener-Holloman parameter, for both material conditions, and a constitutive model was proposed based on the normalized effective stress.

1. Introduction

High temperature applications such that found in power plants for electrical energy generation, oil refineries and petrochemical industries share a common problem; namely ageing of its parts and its consequent degradation or even failure due to their prolonged high temperature-operation. Hence, in order to enhance the reliability, safety and economy of the operation of these plants it is necessary to study the material behavior at high temperature and the accompanying plastic deformation mechanism which can be accomplished through creep or high temperature tensile testing at different temperatures and strain rates. The creep behavior and substructure evolution of newly developed 12% Cr martensitic/ferritic steel in as-received condition and after creep at 650 °C under 130 MPa and 80 MPa was studied by Yadav et al. [1]. In this developed alloy, Ta is added to increase the precipitation kinetics of Z-phase, which forms in the presence of strong carbide formers such as Cr, V and Nb and provide high creep strength. The microstructural and EDX analysis showed that the prior austenite grain boundaries (PAGBs) are decorated with $M_{23}C_6$ carbides and Laves phases. TEM image of the as-received material, revealed the presence of martensitic laths with high dislocation density. The lath boundaries are pinned by the Laves phase particles. In addition, EBSD analysis showed that the sub-grain size increased and the fraction of low angle grain boundaries decreased after creep. Xu et al. [2] investigated the nucleation and growth of $M_{23}C_6$ carbides in a 10% Cr martensite ferritic steel after long-term aging. It was found that most of $M_{23}C_6$ carbides appear on high angle boundaries (HABs) with a misorientation angle of 40–60° and only a small amount of them precipitate at low angle boundaries (LABs)with a misorientation angle of 8–15°. They also reported that the V in $M_{23}C_6$ plays an important role in controlling the coarsening of $M_{23}C_6$ carbides in the period of 70–150 weeks at 650 °C. Pesicka et al. [3] documented the evolution of dislocation densities in tempered martensite-ferritic steels during long-term aging and creep. They confirmed that tempered martensitic-ferritic has a very high initial dislocation density which decreases by a factor of about two during thermal aging (static recovery). In addition, they reported that in long-term creep, dislocation densities steadily decrease and it was found to be homogeneous throughout the microstructure after aging. Yan et al. [4] investigated the creep-resistance property as well as microstructural evolution of 10% Cr ferritic/martensitic heat-resistant steel during creep at 600 °C. It was found that the martensite laths were coarsened with time and eventually developed into subgrains after 8354 h. In addition, Laves phase was observed to grow and cluster along the prior austenite grain boundaries during creep. This would

* Corresponding author. Department of Mechanical Design and Production, Faculty of Engineering, Cairo University, Egypt
E-mail address: edanaf@ksu.edu.sa (E.A. El-Danaf).

http://dx.doi.org/10.1016/j.msea.2017.05.014
Received 28 December 2016; Received in revised form 2 May 2017; Accepted 3 May 2017
Available online 04 May 2017
0921-5093/

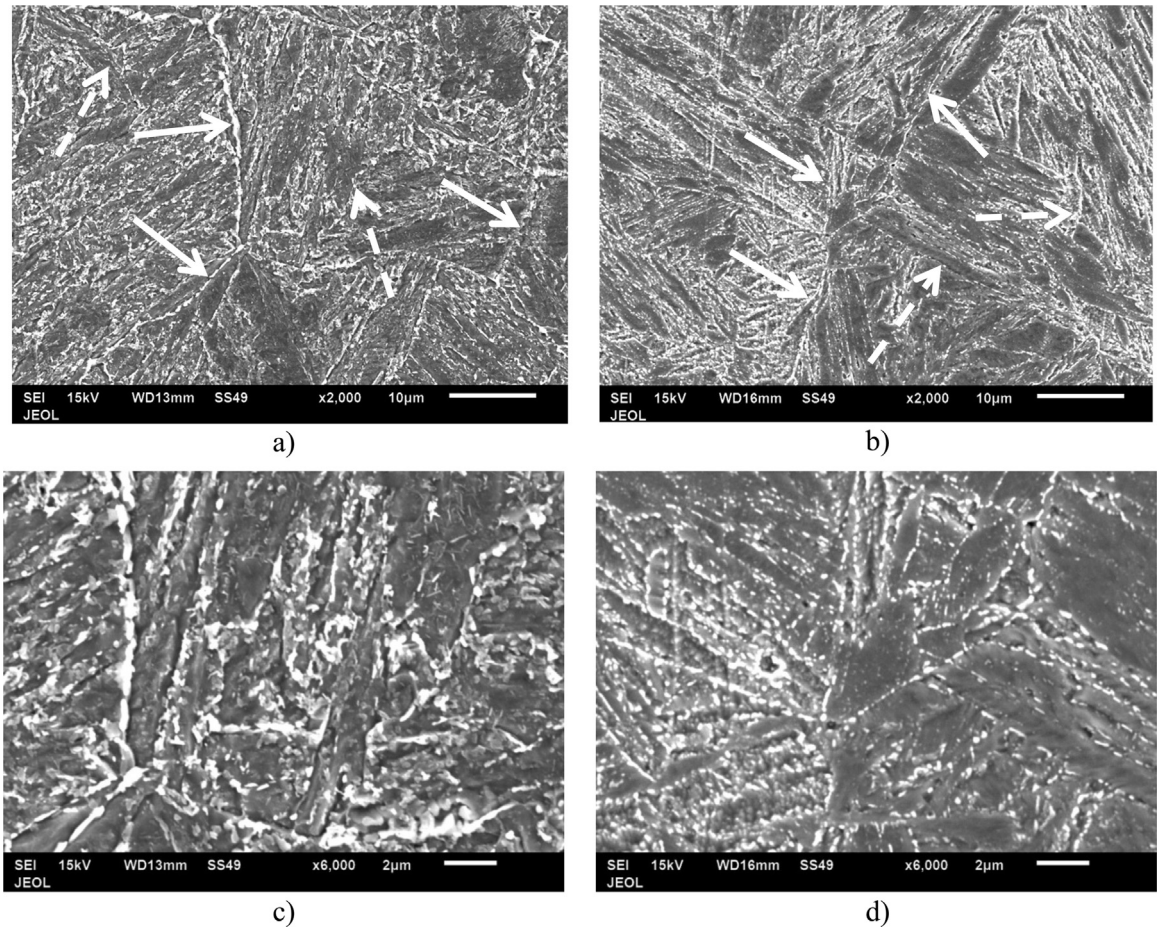

Fig. 1. Comparison between microstructures of retired; left column, and virgin; right column, at different magnifications; a) and b) 2000× and c) and d) ×6000.

greatly reduce the effect of Laves phase on preventing the migration of the lath boundaries, and hence accelerate the lath widening and its evolution to subgrains. Another important effect of the formation of Laves phase is that it consumes the solute atoms, W and Mo, in the steel matrix, so the loss in solution strengthening from W and Mo should be increased along with the increase of the volume fraction of Laves phase. The static recovery of tempered lath martensite during very long-term aging up to 20,000 h. at 650 °C was investigated by Armaki et al. [5], which was found to occur after an incubation period of 1000–2000 h. In addition, the static recovery was reported to be caused by the loss of particle strengthening mainly due to $M_{23}C_6$ precipitates and is controlled by their thermal stability. The stability of $M_{23}C_6$ precipitates is significantly affected by a change of chemical composition in its particles during high temperature exposure. Grain morphology in cold rolled, recrystallize-annealed 9Cr 1Mo commercial grade ferritic steel was investigated by Mungole et al. [6]. The recrystallization annealing up to 100 h at 830 °C exhibited carbide particles embedded in α ferrite grain matrix. The resulting grain sizes were much smaller than those of virgin sample. At longer periods of time over 100 h, the heat treatment resulted in dual phase ferrite-martensite morphology. The recrystallization-annealing at 1030 °C and 1080 °C changed the morphology in complete tempered martensite microstructure significantly, resulting in a harder structure than that of the ferrite. Eggeler et al. [7] investigated the evolution of dislocation densities during heat treatment, long term aging and creep of 12 wt% Cr tempered martensite ferritic steel. It was found that the overall density of free dislocations; which forms in order to facilitate the formation of martensite, decreases during tempering, long term aging and creep. The density of dislocations in low angle boundaries also decreases.

The aim of this work is to study, compare and analyze the behavior of power plant steel in both the as-produced (Virgin) and retired condition at high temperatures and different strain rates to elucidate the dominant deformation mechanism in this temperature and strain rate range.

2. Experimental procedure

The material investigated in this work is 9–12% Cr-power plant steel which is usually used in gas turbine components; namely shrouds. Retired shrouds were selected from a power plant after 30,000 h. in real operation within 550–600 °C, and based on the part number, as-produced shrouds (Virgin) were bought from the same manufacturer. Chemical analysis of both virgin and retired shrouds gave the following chemical composition in wt%; C: 0.328; Cr: 11.55; Ni: 0.196; Mn: 0.256; Si: 0.505; V: 0.0831; Ti: 0.012, which shows that this shroud material belongs to the 9–12% Cr- martensitic- ferritic steel. The microstructure for both materials was studied by EBSD using Oxford HKL system incorporated on a field emission scanning electron microscope (FESEM) 7600 JEOL. For EBSD and SEM imaging, the samples were prepared according to the standard metallographic procedures for sample preparation which include grinding using SiC paper then polished using diamond paste of 1.0 and 0.05 μm then etched with Vilella reagent to reveal the sample's microstructure. For electron back scattered diffraction (EBSD) the samples were polished with colloidal silica as a final step prior to scanning. For microstructural and mechanical testing, round rods of 11 mm diameter were extracted from both shrouds by wire electro-discharge machining (EDM). Tensile specimens were machined according to ASTM E-08. Tensile tests were conducted at temperatures 813, 853, 893 and 933 °K at different strain rates of 1×10^{-3}, 1×10^{-4} and $1\times10^{-5}\,s^{-1}$ using Instron machine

model 3385 H. The machine was equipped with a computer having software through which the load-elongation data were recorded.

3. Results and discussions

3.1. Microstructure

Fig. 1 shows the microstructure of the investigated steel in the as-received (virgin) and retired conditions at different magnifications. In general, the microstructure of both conditions was typically tempered martensite composed of large prior austenite grains [8] (white solid arrows) containing martensite laths (dark) having different orientations at which block boundaries [1,9,10] exist (white dotted arrows) as shown in Fig. 1(a) and (b).

It can be also noted from the same figure that the prior austenite grain size was almost the same with the virgin and retired conditions having the value of about 50–60 μm; as measured by linear intercept method. The reason for this similarity is due to the presence of thermally stable and un-dissolved carbides along the austenite grain boundaries which inhibited the growth of austenite grains, in accordance with what has been reported [11,12]. Furthermore, these carbides precipitated within the martensite laths, at lath boundaries and along prior austenite grain boundaries (PAGBs) forming a continuous network, which is identical to that found in [13–15].

Fig. 1(c) and (d) shows carbides/precipitates (white) at higher magnification, where they were heavily dispersed and eventually interconnected forming clusters within the entire microstructure. Further carbide interpretation, description, characterization and measurements can be found in the author's earlier work [16].

Figs. 2 and 3 present the EBSD results for both virgin and retired conditions, respectively. Fig. 2(a) represent the colored coded map, with grain boundaries defined as misorientation angle exceeding 15°. Fig. 2(b) presents the distribution of grain size with critical misorientation angle taken as 15°, whereas; Fig. 2(c) presents the variation of misorientation angle. The average grain size deduced is about 0.4 μm and the average misorientation angle is 31°. The percentage of LAGBs (boundaries with angle misorientation below 15°) is 48% which is considerably high and indicates the existence of an appreciable amount of dislocations and sub boundaries. The average misorientation angle calculated for the LAGBs is 4.5°, while the average misorientation angle for the HAGBs (high angle grain boundaries) is 45°.

Fig. 3 indicates that after the shroud has experienced high-temperature service (i.e. retired), the grain size increased to about 3.0 μm, and also the average misorientation angle increased to 35°. In addition, the % LAGBs was marginally reduced to 41% on the expense of increasing the % HAGBs. This was expected due to the prolonged high temperature exposure during service which could have led to static recrystallization [12] or at least re-arrangement of dislocations that could lead to well-developed boundaries.

In comparison between virgin and retired conditions, the average of misorientation angle for LAGBs remained almost unchanged, whereas for HAGBs increased marginally from 45° to 55°. Table 1 summarizes the EBSD results for the virgin and retired conditions showing that the major change is in the grain size. These microstructural characteristics are in line with author's earlier published work [16], which was conducted on identical material including retired and virgin conditions.

3.2. Room temperature mechanical properties

Fig. 4 shows the engineering stress-strain plots for both virgin and retired material conditions tested at room temperature. Obviously the virgin condition exhibited higher yield and ultimate tensile strengths as well as less ductility when compared to the retired one. Based on microstructural and EBSD tests results, several reasons may be responsible for this difference. The present authors correlated in an earlier work [16] the hardness values and the accompanying structure with the

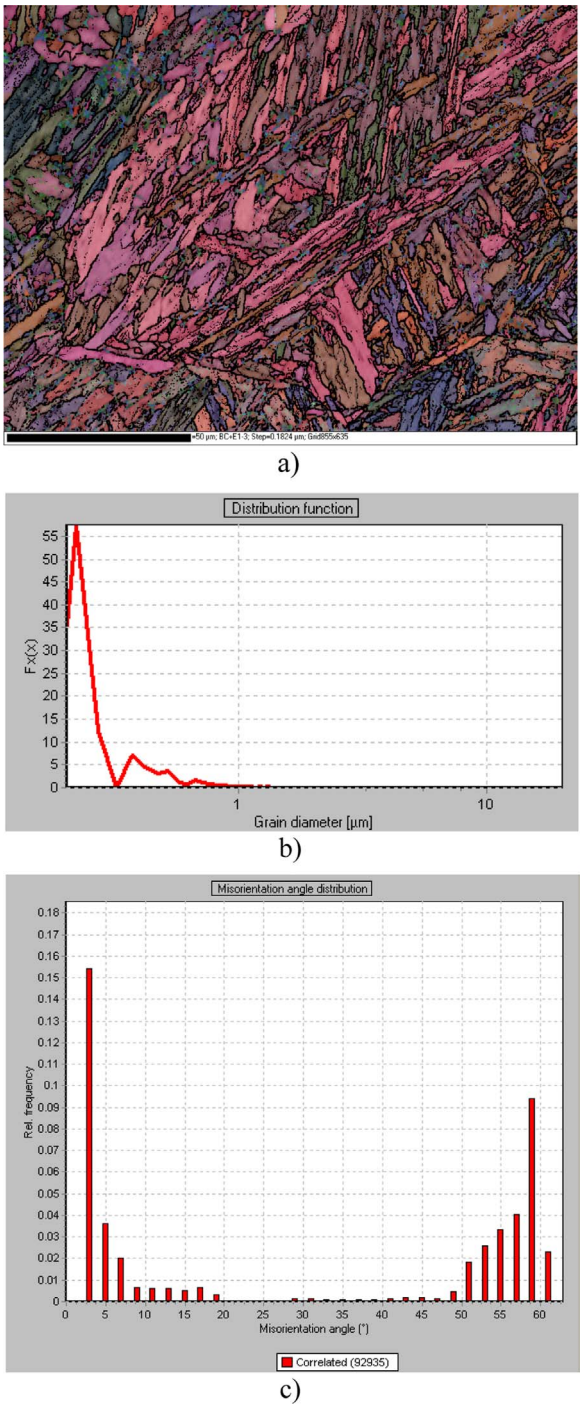

Fig. 2. EBSD results of virgin shroud; a) Colored coded map; b) Grain size distribution with critical misorientation angle taken as 15°; c) Variation of misorientation angle. (For interpretation of the references to color in this figure legend, the reader is referred to the web version of this article.)

ultrasonic properties and it was found to be sensitive to the microstructural constituents, of these two materials conditions, where they reported that the average hardness value of the virgin and retired conditions was reduced from 290 and 180 HV, respectively. In addition the area fraction of carbides found in virgin material was 19.8% whereas it was 15.6% with the retired one, which was attributed to the dissolution and coalescence of these carbides within the matrix. Another reason for the higher strength of the virgin compared to the retired conditions was the percentage of ferrite [softer phase], where in the former condition was 24% whereas it increased to 34% in the later

(a)

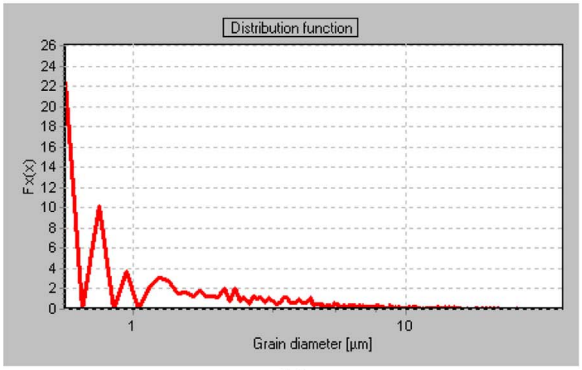

(b)

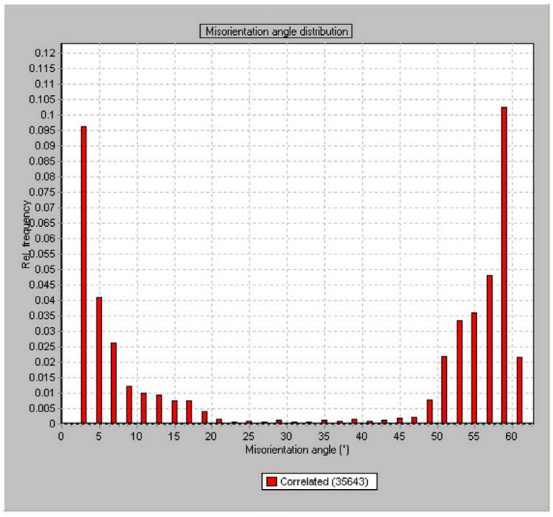

(c)

Fig. 3. EBSD results of retired shroud; a) Colored coded map; b) Grain size distribution with critical misorientation angle taken as 15°; c) Variation of misorientation angle. (For interpretation of the references to color in this figure legend, the reader is referred to the web version of this article.)

one, bearing in mind that martensite [harder phase] coexists with ferrite in both material conditions. The higher hardness and consequently strength in the virgin condition compared to the retired one is referred to the presence of martensite having high dislocation density and also, the higher amount of sub-grain boundaries [17] expressed as percentage of LAGBs as presented in Table 1. These sub-grain boundaries are responsible for microstructural strengthening as well as they act as obstacles to dislocation motion during deformation. Elevated

Table 1
Summary of EBSD results for both virgin and retired conditions.

	Virgin	Retired
Average misorientation angle (°)	31	35
LAGBs (%)	48	41
Average misorientation angle for LAGBs (°)	4.5	5.5
Average misorientation angle for HAGBs (°)	45	55
Average grain size (µm)	0.397	3.0

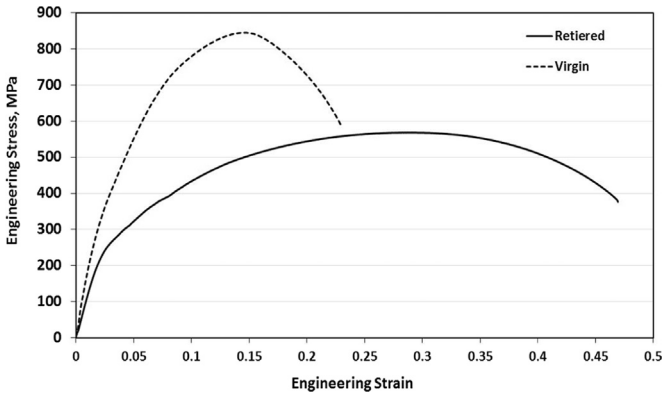

Fig. 4. Room temperature tensile test plots for virgin and retired conditions.

temperature exposure during service for the retired condition caused a reduction in the dislocation density, reduction in the fraction of sub-boundaries and less dispersion and dissolution of carbides, all of which were reflected on the reduction of hardness and strength.

3.3. High temperature tensile tests

The stress dependence of secondary creep rate at low stress levels is usually given by the power law relation (Eq. (1)) [18]:

$$\dot{\varepsilon} = A\sigma^n \tag{1}$$

where $\dot{\varepsilon}$ is the steady state strain rate, A is a temperature dependent constant, n is the stress exponent and σ is the steady state flow stress.

At high stress levels, the stress dependence of creep rate is given by an exponential behavior (Eq. (2)) [18]:

$$\dot{\varepsilon} = A' \exp \beta\sigma \tag{2}$$

Eqs. (1) and (2) can be satisfied by a single stress function that can be used when there is an abrupt change in the controlling deformation mechanism, within the temperature range studied. This function is given by (Eq. (3)) [18]:

$$\dot{\varepsilon} = A''(\sinh \alpha\sigma)^n \tag{3}$$

where α and β are constants with units of MPa^{-1}.

In the present investigation, true stress – true strain response was documented at four temperatures 813, 853, 893 and 933 K at three strain rates of 10^{-3}, 10^{-4} and $10^{-5}\,s^{-1}$. Figs. 5 and 6 present two examples of the true stress–true strain responses at 853 and 893 K respectively, for the virgin and retired conditions.

Depicting the maximum flow stress for each testing condition and plotting them against strain rate in a double logarithmic plot obeying the power law equation; Eq. (1), gives the results presented in Fig. 7(a) and (b) for the virgin and retired conditions, respectively.

Within the temperature range investigated, the stress exponent exhibited in the virgin condition was in the range from 12.5 to 15.5 which points towards power law break down regime. An average stress exponent (n) value of 13.5 will be used in further analysis for this material condition. Whereas, for the retired condition, the stress exponent exhibited an average value of 11.2 in the temperature range of 813–893 K, while at 933 K it exhibited a value of about 7. This can be

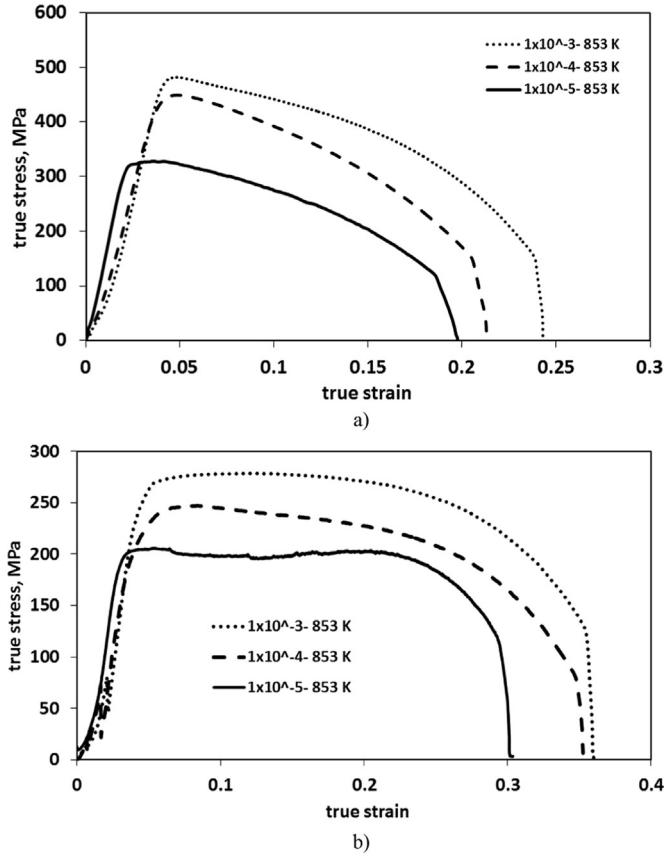

Fig. 5. True stress–true strain responses at 853 K for; a) virgin and b) retired conditions.

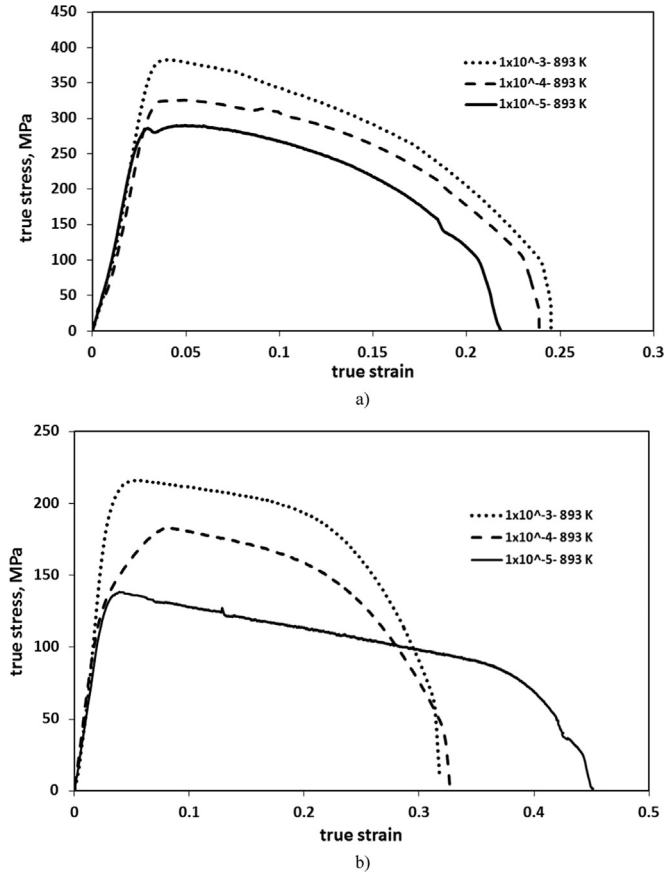

Fig. 6. True stress–true strain responses at 893 K for; a) virgin and b) retired conditions.

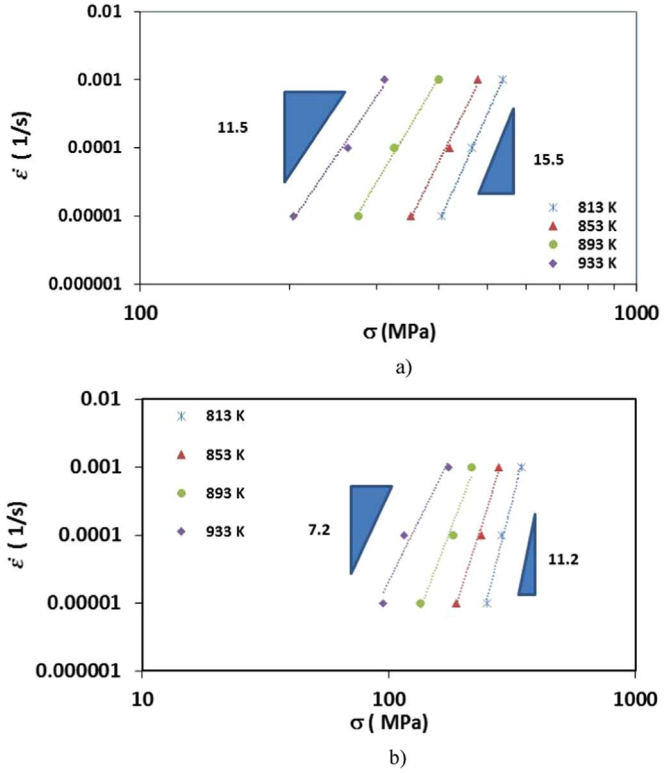

Fig. 7. Double logarithmic plot for maximum flow stress versus strain rate for a) Virgin and b) Retired conditions at different testing temperatures.

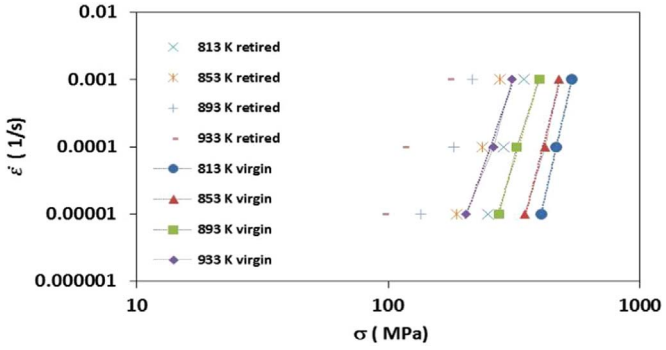

Fig. 8. Stress dependence on strain rate for the virgin (lines with symbols) and retired conditions (symbols only).

interpreted as a transition in the deformation controlling mechanism in the range of temperatures tested. Fig. 8 presents a comparison of the stress dependence on strain rate for the virgin (lines with symbols) and retired conditions (symbols only). By observing the horizontal shift for same testing temperature, it reveals, with no doubt, the superiority of the virgin material over the retired one, in the range of temperatures and strain rates tested.

Since the data for the virgin condition was all explicitly lying in the power law breakdown regime with an average stress exponent of 13.5, the data will be re-plotted according to Eq. (2). Strain rate was plotted against stress on a semi- logarithmic plot as in Fig. 9 to calculate the average value of β which turns out to be 0.037.

The apparent activation energy was calculated for the virgin condition based on Eq. (2), after being manipulated for the constant strain rate to the following equation:

$$\sigma = \ln A' + \frac{Q_a}{\beta R} \cdot \frac{1}{T} \tag{4}$$

where Q_a is the apparent activation energy and R is the universal gas

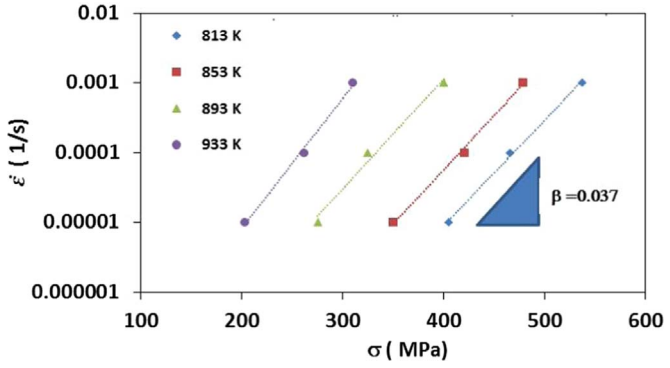

Fig. 9. Strain rate versus stress plot for β calculation of the virgin condition.

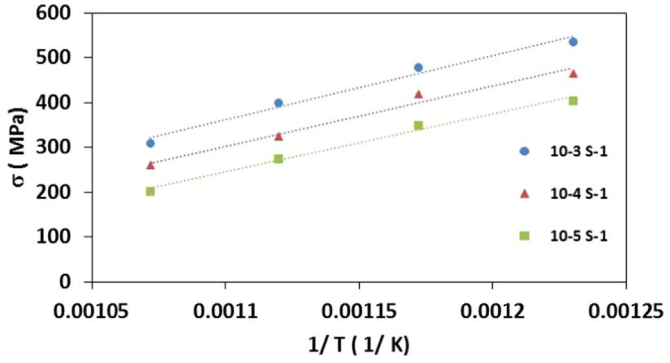

Fig. 10. Stress versus temperature reciprocal for apparent activation energy calculation.

constant.

By plotting stress against the reciprocal of temperature in a double linear plot, as shown in Fig. 10, the apparent activation energy was calculated to be 300 kJ/mol. The apparent activation was, also, re-evaluated based on the power law behavior after being manipulated into the following form:

$$Q_a = nR\left[\frac{\partial \ln \sigma}{\partial(1/T)}\right]_{\dot{\varepsilon}} \tag{5}$$

Thus by plotting stress against the reciprocal of temperature on a semi logarithmic plot, and taking an average value of 13.5 for n, the apparent activation energy was calculated to be 414 kJ/mol (not shown here).

The high stress exponent and the high activation energy point towards the possibility of threshold behavior. The threshold-stress behavior is characterized by two points [19,20]: (i) a high value of stress exponent, n that continuously increases with decreasing stress and (ii) a high value of activation energy above that reported for self-diffusion. The threshold-stress concept arises due to the interaction between fine particles and dislocation. Under the presence of threshold stress, the applied stress is replaced by an effective stress, $(\sigma-\sigma_o)$. The threshold stress values were identified through the following equation.

$$\dot{\varepsilon}^{(\frac{1}{n})} = A(\sigma - \sigma_o) \tag{6}$$

The value of n was substituted for 3 (viscous glide), 5 (dislocation climb) and 7 (pipe diffusion) and best fit was achieved with 7, which is correlated to low temperature climb known as pipe diffusion where the deformation is controlled by diffusion of atoms through dislocation cores. Fig. 10 presents $\dot{\varepsilon}^{(\frac{1}{7})}$ versus stress on a double linear plot. The points where the lines in Fig. 11 intersect the zero strain rate represent the threshold stress values. The values σ_o were depicted as a function of the temperature and has the values of 89, 142, 215, 258 MPa for the temperatures of 933, 893, 853 and 813 K, respectively.

Based on the threshold concept, Eq. (1) was modified such that this equation when written in the normalized form and the stress was

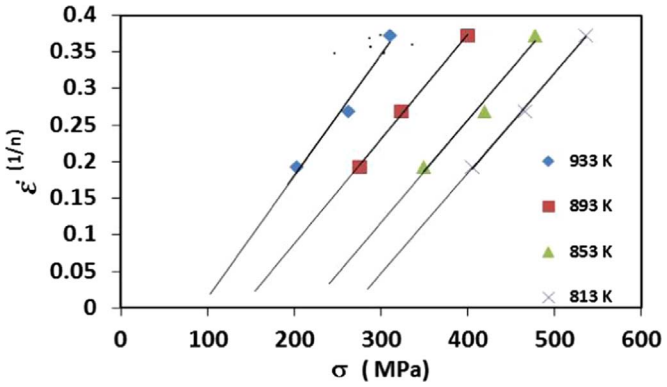

Fig. 11. Threshold stress versus $\dot{\varepsilon}^{(\frac{1}{7})}$ at different testing temperatures for the virgin condition.

substituted for the effective stress is given by:

$$\frac{\dot{\varepsilon}kT}{DGb} = A_o\left(\frac{\sigma - \sigma_o}{G}\right)^n \tag{7}$$

where k is Boltzmann's constant, b is the magnitude of Burgers vector, A_o is a dimensionless constant, Q_t is the true activation energy for the diffusion process that controls the deformation mechanism, n_t is the true stress exponent and $(\frac{\sigma-\sigma_o}{G})$ is the effective normalized stress.

Shear modulus of elasticity (G) as a function of temperature was deduced from the following equation E (GPa) $= 445.2 - (899.6*0.001*T) + (1098.8*(0.001*T)^2) - (494.5*(0.001*T)^3)$ [21].

with

$$D = D_o \exp\left(\frac{-Q_t}{RT}\right) \tag{8}$$

where D_o is a frequency factor. At constant strain rate, Eq. (7) can be rearranged in the form

$$\exp\left(\frac{Q_t}{RT}\right) = C\left(\frac{G}{T}\right)\left(\frac{\sigma - \sigma_o}{G}\right)^{n_t} \tag{9}$$

where C is a constant. Taking the natural logarithm of Eq. (9) and differentiating with respect to $(\frac{1}{T})$, the value of Q_t can be written as

$$Q_t = R\frac{\partial \ln\left[\frac{G}{T}\left(\frac{\sigma - \sigma_o}{G}\right)^{n_t}\right]}{\partial\left(\frac{1}{T}\right)} \tag{10}$$

Eq. (10) is used to calculate the true activation energy (Q_t) by plotting $\log[\frac{G}{T}(\frac{\sigma-\sigma_o}{G})^7]$ vs $(1/T)$ as shown in Fig. 12. The value of Q_t was determined at three various strain rates in the temperature range of 813–933 K. As shown in figure, the data points fall on segments of

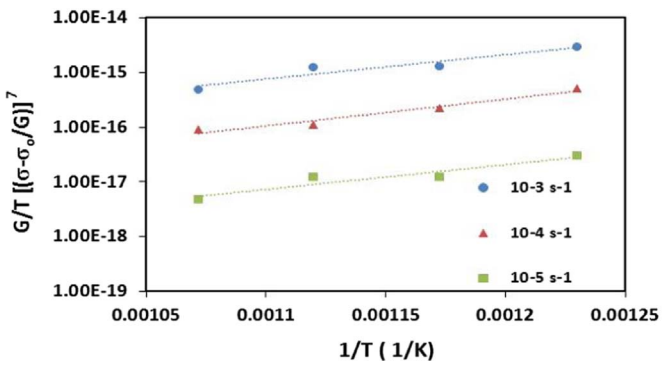

Fig. 12. Determination of true activation energy Q_t of the virgin condition at three strain rates within the temperature range 813–933 K.

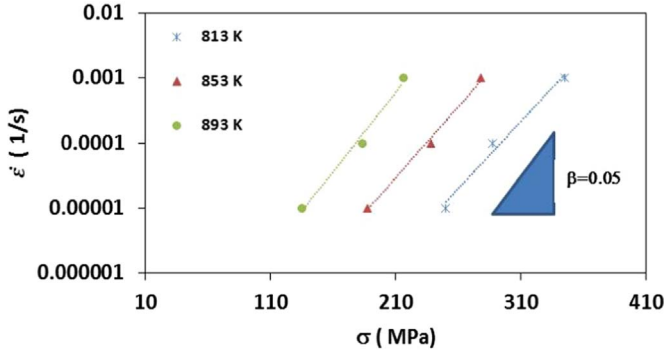

Fig. 13. Strain rate versus stress plot for β calculation of the retired condition.

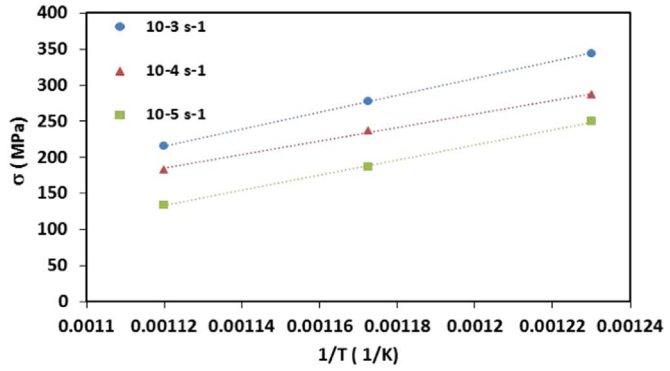

Fig. 14. Determination of true activation energy Q_t of the retired condition at three strain rates within the temperature range 813–933 K.

parallel straight lines giving Q_t a constant value independent of strain rate. The average value of Q_t was calculated as 94 kJ/mol. This value is very close to 60% of lattice diffusion in ferrite as expected for low temperature climb.

For the retired condition, the three temperatures that exhibited power law break down were plotted according to Eq. (2) as in Fig. 13, and the average β value was calculated to be 0.05. The apparent activation energy was calculated according to Eq. (4), as shown in Fig. 14, to be 415 kJ /mol.

For the retired condition, since the data ranged from power law beak down with an average exponent of 11.2 to power law with exponent of 7, the hyperbolic equation; Eq. (3), will be used to express the whole range of data. The value of β′ was calculated according to Eqs. (11) and (12) and the value of α' was calculated to be β′/n, where, n being the stress exponent depicted at high temperature/low stresses or power law region, which was about ~7.

$$\dot{\varepsilon} = A' \exp\ \beta'\left(\frac{\sigma}{G}\right) \tag{11}$$

$$\ln\ \dot{\varepsilon} = \ln\ A' + \beta'\left(\frac{\sigma}{G}\right) \tag{12}$$

From Fig. 15, β′ was deduced to be 3200 and thus the value of α′ was calculated as 458.

Using the hyperbolic function in a normalized manner, Eq. (13) was used. The apparent activation energy equation was calculated as 440 kJ mol^{-1} as depicted from Fig. 16, which was plotted according to Eq. (14) at constant strain rate.

$$\dot{\varepsilon}\exp\frac{Q}{RT} = \frac{AD_oGb}{KT}\left[\sinh\left(\alpha'\frac{\sigma}{G}\right)\right]^n \tag{13}$$

$$\frac{Q}{R}\cdot\frac{1}{T} = \ln\frac{AD_ob}{K} + \ln\frac{G}{T}\left[\sinh\left(\alpha'\frac{\sigma}{G}\right)\right]^n \tag{14}$$

The high value of the stress exponent and the high activation energy point towards the existence of threshold behavior.

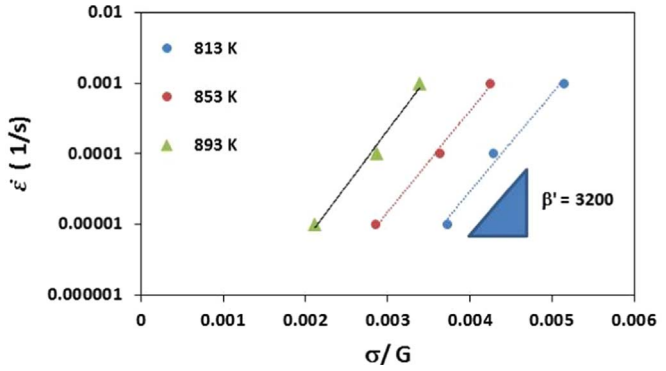

Fig. 15. Strain rate vs normalized stress in the temperature range of 813–893 K for the retired condition.

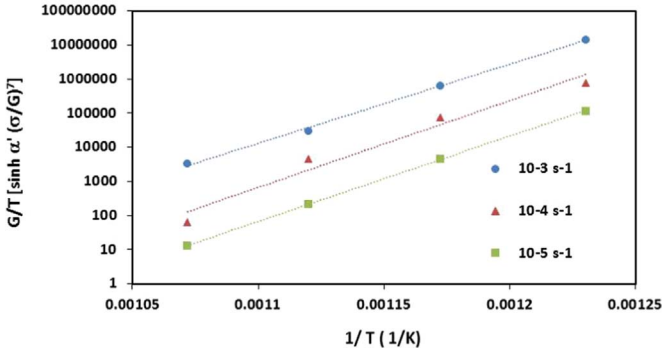

Fig. 16. Calculation of apparent activation energy for the retired condition by plotting $\frac{G}{T}[\sinh\left(\alpha'\frac{\sigma}{G}\right)]^7$ vs 1/T on a semi logarithmic plot.

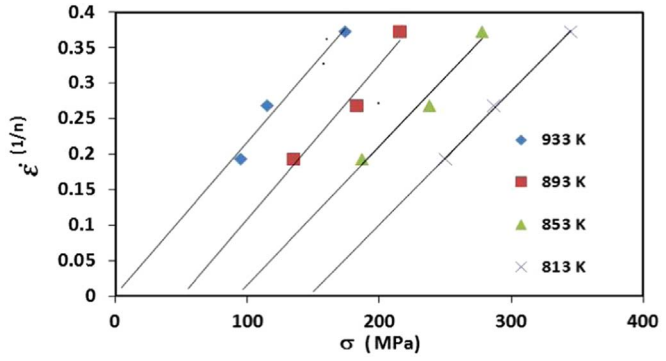

Fig. 17. Threshold stress versus $\dot{\varepsilon}^{(\frac{1}{7})}$ at different testing temperatures for the retired condition.

Fig. 17 represent the plot of $\dot{\varepsilon}^{(\frac{1}{7})}$ versus stress and the threshold stress was calculated as zero, 49, 89 and 145 MPa at temperatures of 933, 893, 853 and 813 K, respectively. As expected the threshold at 933 K is zero, because the stress exponent, at this particular temperature, had a value of 7 initially.

The true activation energy was calculated according to Eq. (15) and through Fig. 18 to be 117 kJ mol^{-1} which is again close to 60% of lattice diffusion in ferrite.

$$\dot{\varepsilon}\exp\frac{Q}{RT} = \frac{AD_oGb}{KT}\left[\sinh\left(\alpha'\frac{\sigma-\sigma_O}{G}\right)\right]^n \tag{15}$$

To consolidate the data for the virgin and retired conditions, Zener-Hollomon parameter, defined by Eq. (16), is used

$$Z = \dot{\varepsilon}\exp\left(\frac{Q_t}{RT}\right) = B\left(\frac{\sigma-\sigma_o}{G}\right)^{n_t} \tag{16}$$

Fig. 19 presents the variation of Zener-Hollomon parameter vs. the

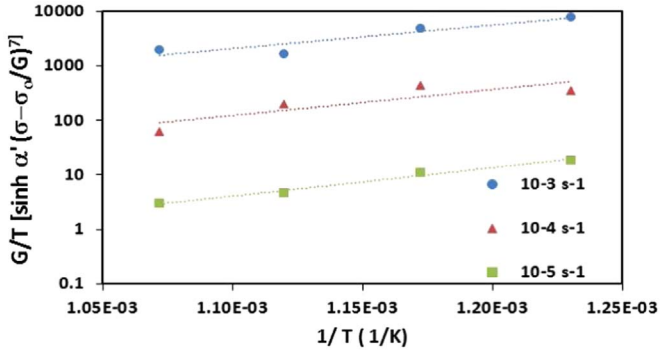

Fig. 18. Semi logarithmic plot of $\frac{G}{T}[\sinh\left(\alpha'\frac{\sigma-\sigma_O}{G}\right)]^7$ vs 1/T for constant strain rates, to calculate the true activation energy.

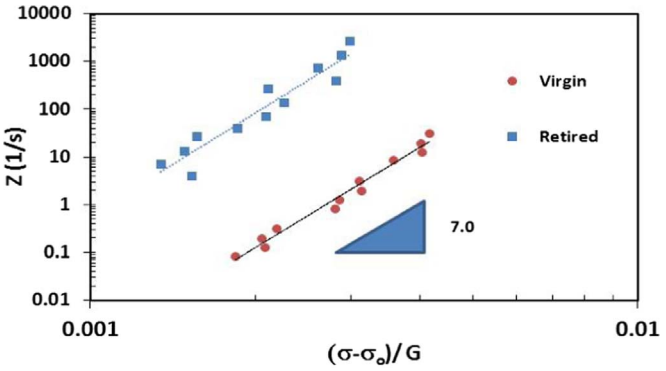

Fig. 19. The relation between Zener-Hollomon parameter versus the normalized effective stress.

normalized effective stress ($\frac{\sigma-\sigma_o}{G}$) using double logarithmic scale for the virgin and retired conditions. Worth mentioning that all points coalesced on a segment of a straight line with a slope of about 7.

For the retired condition the equation is as follows:

$$Z = 1E + 21\left(\frac{\sigma-\sigma_o}{G}\right)^{7.1}$$

For the virgin condition the equation is as follows:

$$Z = 9E + 17\left(\frac{\sigma-\sigma_o}{G}\right)^{6.98}$$

It is obvious that a higher value of Z is attained for the retired condition for the same normalized effective stress values.

4. Conclusions

In the present work power plant steel (9–12% Cr) having two conditions; namely as-produced and retired, were studied, compared and analyzed with respect to their behavior at high temperatures and different strain rates in order to elucidate the dominant deformation mechanism in this temperature and strain rate range. Based on the results obtained the following conclusions can be drawn:

- Comparison between the microstructure of the retired and virgin conditions using EBSD revealed that average misorientation angle as well as the average grain size increased whereas the LAGBs was reduced for the former condition.
- Long temperature service at high temperatures causes softening and loss of strength when compared to the as-produced material both at room temperature as well as at high temperatures.
- Within the temperature range investigated, the value of the stress exponent with the virgin condition was from 11.5 to 15.5, pointing towards power law break down regime. Whereas, for the retired condition, the stress exponent exhibited an average value of 11.2 in the temperature range of 813–893 K, while at 933 K it exhibited a value of about 7.
- The apparent activation energy of the virgin condition was calculated to be 300 kJ/mol whereas for the retired condition it was 415 kJ/mol, along with the high stress exponents; point toward the possibility of threshold behavior that arises from the interaction of dislocations with second phases and carbides.
- Analysis was made based on threshold concept where the effective stress was calculated and true activation energies was calculated as 94 and 117 kJ/mol for the virgin and retired conditions, respectively. These values along with the true stress exponent of 7 point towards that low temperature climb known as pipe diffusion where the deformation is controlled by diffusion of atoms through dislocation cores could be the controlling deformation mechanism.

Acknowledgment

This work was supported by the Research Center, College of Engineering, Deanship of Scientific Research, King Saud University.

References

[1] Surya Deo Yadav, Szilvia Kalácska b, M.ária Dománková c, David Canelo Yubero a, Roland Resel, István Groma, Coline Beal, Bernhard Sonderegger, Christof Sommitsch, Cecilia Poletti, Evolution of the substructure of a novel 12% Cr steel under creep conditions, Mater. Charact. 115 (2016) 23–31.
[2] Y. Xu, X. Zhang, Y. Tian, C. Chen, Y. Nan, H. He, M. Wang, Study on the nucleation and growth of $M_{23}C_6$ carbides in a 10% Cr martensite ferritic steel after long-term aging, Mater. Charact. 111 (2016) 122–127.
[3] J. Pesicka, A. Aghajani, Ch Somsen, A. Hartmaier, G. Eggeler, How dislocation substructures evolve during long-term creep of a 12% Cr tempered martensitic ferritic steel, Scr. Mater. 62 (2010) 353–356.
[4] Ping Hu, Wei Yan, Wei Sha, Wei Wang, Yiyin Shan, Ke Yang, Microstructure evolution of a 10Cr heat-resistant steel during high temperature creep, J. Mater. Sci. Technol. 27 (4) (2011) 344–351.
[5] H. Ghassemi-Armaki, R.P. Chen, K. Maruyama, M. Yoshizawa, M. Igarashi, Static recovery of tempered lath martensite microstructures during long-term aging in 9–12% Cr heat resistant steels, Mater. Lett. 63 (2009) 2423–2425.
[6] M.N. Mungole, Gadadhar Sahoo, S. Bhargava, R. Balasubramaniam, Recrystallized grain morphology in 9Cr 1Mo ferritic steel, Mater. Sci. Eng. A 476 (2008) 140–145.
[7] J. Pesicka a, A. Dronhofer b, G. Eggeler, Free dislocations and boundary dislocations in tempered martensite ferritic steels, Mater. Sci. Eng. A 387–389 (2004) 176–180.
[8] D.R.G. Mitchell, C.J. Moss, Characterization of seven power-generating turbine rotors using microscopy-based techniques, J. Mater. Eng. Perform. JMEPEG 7 (1998) 621–631.
[9] Dong-Yeol, Kim, Hak-Joon, Kim, Sung-Jin, Song, Bum-Joon, Kim, Byeong-Soo, Lim, Review of quantitative nondestructive evaluation, in: D.O. Thompson, D.E. Chimenti (Eds), Evaluation of isothermal aged 9Cr-2W steel using ultrasound, CP975, Vol. 27, American Institute of Physics. 978-0-7354-0494-6/08.
[10] Feng-shi Yin, Woo-sang Jung, Soon-hyo Chung, Microstructure and creep rupture characteristics of an ultra-low carbon ferritic/martensitic heat-resistant steel, Scr. Mater. 57 (2007) 469–472.
[11] V. Thomas Paul, S. Saroja, M. Vijayalakshmi, Microstructural stability of modified 9Cr–1Mo steel during long term exposures at elevated temperatures, J. Nucl. Mater. 378 (2008) 273–281.
[12] H. Ghassemi-Armaki, R.P. Chen, K. Maruyama, M. Yoshizawa, M. Igarashi, Static recovery of tempered lath martensite microstructures during long-term aging in 9–12% Cr heat resistant steels, Mater. Lett. 63 (2009) 2423–2425.
[13] J.án Michel, Marián Buršák, Marek Vojtko, Microstructutre and mechanical properties degradation of Cr Mo creep resistant steel operating under creep conditions, Mater. inžinierstvo Mater. Eng. 18 (2011) 57–62.
[14] G. Golanski, J. Slania, Effect of different heat treatments on microstructure and mechanical properties of the martensitic GX12CrMoVNbN9-1 cast steel, Arch. Metall. Mater. 58 (1) (2013), http://dx.doi.org/10.2478/v10172-012-0145-x.
[15] Yinzhong Shen, Xiaoling Zhou, Tiantian Shi, Xi Huang, Zhongxia Shang, Wenwen Liu, Bo Ji, Zhiqiang Xu, Sigma phases in an 11%Cr ferritic/martensitic steel with the normalized and tempered condition, Mater. Charact. 122 (2016) 113–123.
[16] Magdy M. El Rayes, Ehab A. El-Danaf, Abdulhakim A. Almajid, Characterization and correlation of mechanical, microstructural and ultrasonic properties of power plant steel, Mater. Charact. 100 (2015) 120–134.
[17] A. Aghajani, Ch Somsen, G. Eggeler, On the effect of long-term creep on the microstructure of a 12% chromium tempered martensite ferritic steel, Acta Mater. 57 (2009) 5093–5106.
[18] Frank Garofalo, Fundamentals of Creep and Creep-Rupture in Metals, Macmillan Series in Materials Science, 1965.
[19] Ehab A. El-Danaf, Mahmoud Soliman, Abdulhakim Almajid, Effect of solution heat treatment on the hot workability of Al-Mg-Si alloy, J. Mater. Manuf. Process. 24 (2009) 637–644.
[20] E.A. El-Danaf, A.A. Almajid, M.S. Soliman, High-temperature deformation and ductility of modified 5083 Al alloy, J. Mater. Eng. Perform. 17 (4) (2008) 572–579.
[21] [⟨http://www.engineeringtoolbox.com/young-modulus-d_773.html⟩].